Hybrid Proton and Electron Transport in Peptide Fibrils

*Moran Amit, Sagi Appel, Rotem Cohen, Ge Cheng, Ian W. Hamley, and Nurit Ashkenasy**

Protons and electrons are being exploited in different natural charge transfer processes. Both types of charge carriers could be, therefore, responsible for charge transport in biomimetic self-assembled peptide nanostructures. The relative contribution of each type of charge carrier is studied in the present work for fibrils self-assembled from amyloid-β derived peptide molecules, in which two non-natural thiophene-based amino acids are included. It is shown that under low humidity conditions both electrons and protons contribute to the conduction, with current ratio of 1:2 respectively, while at higher relative humidity proton transport dominates the conductance. This hybrid conduction behavior leads to a bimodal exponential dependence of the conductance on the relative humidity. Furthermore, in both cases the conductance is shown to be affected by the peptide folding state under the entire relative humidity range. This unique hybrid conductivity behavior makes self-assembled peptide nanostructures powerful building blocks for the construction of electric devices that could use either or both types of charge carriers for their function.

1. Introduction

Conductive and semiconductive organic materials have been intensively investigated and exploited in advanced electronic devices.[1] Inspired by the high efficiency of charge transport in biological systems, the possibility of introducing proteins, instead of synthetic polymers and small organic molecules, has been suggested. For example, proteins have been used as transistor channels,[2] as well as bridges in molecular junctions.[3] The use of man-made peptides instead of natural proteins has been proposed in order to combine the advantages of both natural and synthetic organic materials. Indeed, high efficiency electron transport has been observed through molecular junction containing helical peptides.[4] In a recent work we have demonstrated control of electrical characteristics of molecular junctions by the conformation of synthetic coiled coil proteins that were used as bridges in such junctions.[5]

Beyond the use of peptides as bridges in molecular junctions, long range conduction channels have been realized utilizing self-assembly of peptides into nanotubes and nanofibers.[6] Ashkenasy and co-workers have shown in the past that peptide self-assembly can be used to promote stacking of non-natural aromatic side chains attached to them, leading to the formation of delocalized electron energy levels.[7] We have recently shown that for peptides derived from amyloid-β sequence, which assemble into elongated nanofibrils, the introduction of two non-natural 2-thienylalanine (2-Thi) amino acids instead of the diphenylalanine domain that is part of the natural sequence, improves the conductance under low pressure conditions.[8] This could be expected due to the electronic conducting nature of the thiophene side chain, which makes it a common choice for the synthesis of conductive polymers.[9] However, since chains of hydrogen bonds and the presence of hydrogen donating and accepting groups, such as carboxylic acid and amino groups, may facilitate effective proton conduction channels by the Grotthuss mechanism, the precise identity of charge carriers in such β-sheet assemblies is not clear.[10] Indeed, since the early days of studying charge transport through proteins in the solid state, there has been a great debate on whether electron or proton transport dominates the conduction.[11] This question is of critical importance for determining the possible applications of such nanostructures;[12] electronic conduction in self-assembled peptide fibrils may lead to diverse electronic and optoelectronic applications;[13] whereas proton conducting peptide assemblies can be used to replace synthetic polymer networks in applications such as supercapacitors,[14] rechargeable batteries,[15] and fuel cells.[16] Furthermore, since both proton donating and proton accepting groups can be incorporated in the peptide framework, the fabrication of protonic electric devices such as protonic transistors and diodes can be materialized, as recently demonstrated for bio-inspired polysaccharides.[17] In the present work we combine AC and DC measurements to monitor electrical characteristics of self-assembled networks based on thiophene containing amyloid-β

M. Amit, S. Appel, R. Cohen, Prof. N. Ashkenasy
Department of Materials Engineering
Ben-Gurion University of the Negev P.O.B. 653
Beer-Sheva 84105, Israel
E-mail: nurita@bgu.ac.il
Prof. N. Ashkenasy
The Ilse Katz Institute for Nanoscale Science and Technology
Ben-Gurion University of the Negev P.O.B. 653
Beer-Sheva 84105, Israel
Dr. G. Cheng,[+] Prof. I. W. Hamley
Department of Chemistry
University of Reading
Reading RG6 6AD, UK
[+]Present address: Department of Chemistry, University of Liverpool, Crown Street, Liverpool L69 7ZD, UK

DOI: 10.1002/adfm.201401111

derived peptides.[8,18] We show that under high relative humidity conditions the network behaves as a proton exchange membrane. However, a bimodal exponential dependence of the conductance on the relative humidity is observed and is related to hybrid electrons and protons transport. Furthermore, we show that under the entire relative humidity range the conductance is affected by the folding state of the peptide nanostructures.

2. Results and Discussion

2.1. Peptide Network Morphology

(2-Thi)(2-Thi)VLKAA (Figure S1) fibril network was chosen in this work for studying the nature of charge carriers of self-assembled peptide fibril networks. These peptide fibrils were used due to their higher conductance with respect to that of fibrils based on the "native" amyloid-β peptide segment, AAKLVFF.[8] Drop- casting the fibrils from 0.3 mM methanol solution resulted in the formation of a network of nanofibers both for freshly prepared solutions and for solutions aged for one week (**Figure 1**). Two types of twisted fibers, with typical diameter in the range of 13 ± 5 nm and 45 ± 10 nm, and length of several micrometers, were observed in both cases. High magnification image of the aged solution indicated the formation of twisted fibers with a pitch of about 0.2 μm (Figure S2). However, some of the material was found to be only partially folded for the freshly prepared sample, and appeared as sheets with an area of a few μm^2 (marked by an arrow in Figure 1a and dark areas in Figure 1c). Upon aging in solution the folding process was allowed to complete, resulting in a more homogeneous network, as was manifested by the disappearance of these extended sheets (Figure 1 b and d).

2.2. Electrical Behavior at High Relative Humidity

Proton transport is greatly affected by the presence of water molecules. This is since water induces protonation processes in which protons are transferred from the organic scaffold to a water molecule to form H_3O^+ ions, or from the water molecule to the organic scaffold, resulting in solvated OH^- ions. Both processes introduce protonic-type charge carriers to the system.[19] This process becomes more efficient with an increase in the relative humidity due to an increase in the permittivity, ε, which lowers the activation energies required to detach the charge carriers from the organic scaffold. This results in an exponential dependence of the charge carriers density, n, on ε, as indicated by Equation (1):[19a,20]

$$n = n_0 \exp\left(\frac{-e^2}{2\varepsilon_{(RH)} r R_B T}\right) \quad (1)$$

where n_0 is the effective protonic charge carriers density at 0% relative humidity, e is the electron charge, r is the average equilibrium distance between charge species, R_B is the gas constant, and T is the absolute temperature.

Equation (1) implies that proton transport should be more dominant at elevated humidity conditions. Hence, initial transport measurements were conducted at 80% relative humidity. Current-voltage (I–V) traces revealed a purely Ohmic behavior for both freshly prepared and aged peptide networks (**Figure 2**a), and for a reference bare sample after Piranha treatment without the presence of a peptide network. This linear behavior indicates that under such measurement conditions water dissociation does not occur.[21] A single slope linear dependence was found also in the log-log plots of the I–V data (inset of Figure 2a), indicating that possible contribution of contamination ions is negligible.[11e] This is expected due to the high purity of peptides and solvents used for samples' preparation, and the low electric fields used in the measurements.[11e,22]

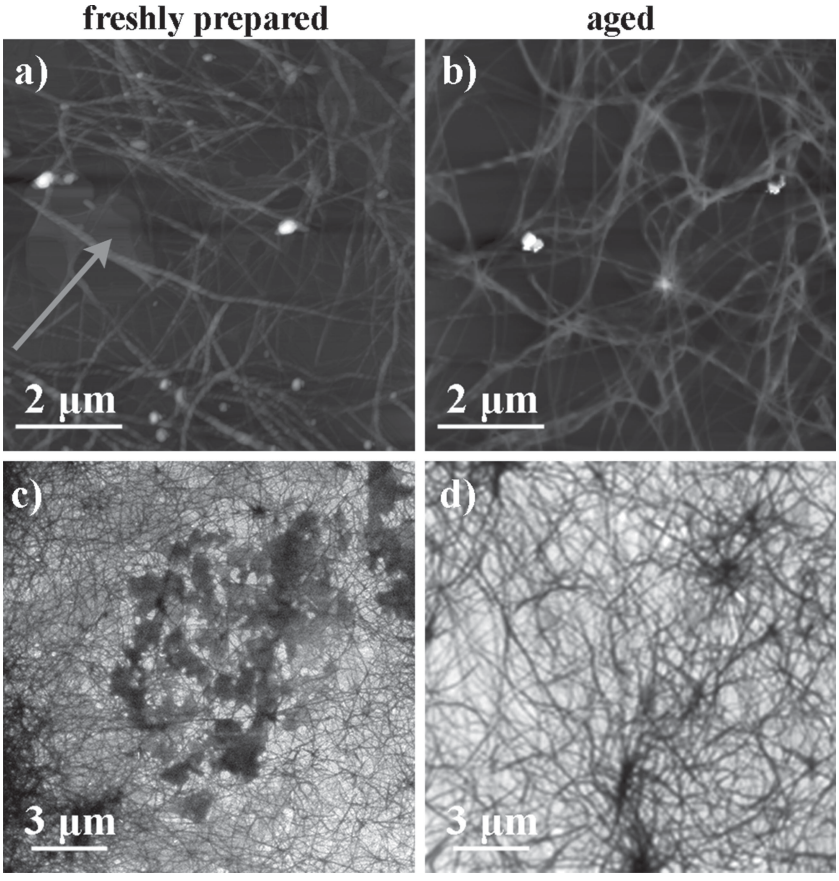

Figure 1. Morphology of (2-Thi)(2-Thi)VLKAA self-assembled peptide networks. Atomic force microscopy (AFM) topography (a, b) (z-scale 200 and 140 nm, respectively) and scanning electron microscopy (SEM) (c, d) images of 0.3 mM (2-Thi)(2-Thi)VLKAA self-assembled in Methanol. Samples were prepared by drop-casting from a, c) fresh, and b, d) one week aged solutions. The arrow in panel a) marks an unfolded peptide Sheet. Such sheets appear as dark areas in c).

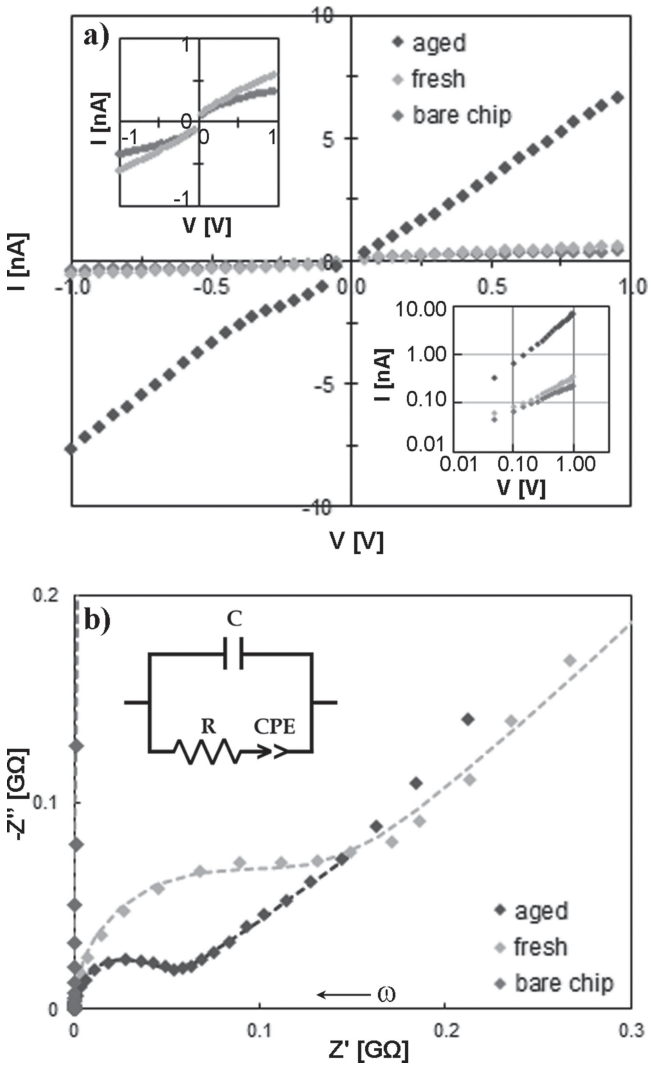

Figure 2. Electrical characteristics of fresh and aged peptide networks at elevated relative humidity. a) *I–V* curves under 80% relative humidity. Data of freshly prepared network and of the reference sample (chip without a peptide network) was recorded on chips with 300 μm wide electrodes, while data of samples prepared from one week aged solutions was recorded on chips with 500 μm wide electrodes and was normalized by a factor of 0.6 in order to compare the results. Zoom on the *I–V* curves of a fresh network and bare chip appears in the inset at the top left. The data is plotted in logarithmic scale in the bottom right inset. b) Nyquist plots acquired from impedance spectroscopy measurements conducted on chips with 300 μm wide electrodes at 75% relative humidity. Inset shows the equivalent electric circuit used for impedance spectroscopy data fitting. Dashed lines represent the fitting results obtained for the suggested equivalent circuit. An arrow indicates the direction of increasing measurement frequency (ω).

The peptide networks' conductance, *G*, was extracted from the slope of the *I–V* curves. The conductance of the freshly prepared sample was found to be 0.63 ± 0.01 nS, ~35% larger than that of the bare reference sample. An order of magnitude increase in the conductance to a value of 7.13 ± 0.05 nS was found for a network prepared from an aged peptide solution. These results indicate that complete folding of the peptide into fibrils improves the conductance.

Impedance spectroscopy measurements were conducted in order to confirm the dominance of proton transport. Nyquist plots of both freshly prepared and aged peptide networks at relative humidity of 75% revealed a shape of a high frequency semi-circle with a low frequency slope (Figure 2b). This type of behavior is typical for ionic conductive materials.[23] Indeed, the impedance spectroscopy data could be fitted using an electric circuit shown in the inset of Figure 2b, which is typically used for modeling proton exchange membranes.[24] In this circuit *R* corresponds to the bulk resistance of the system, and the constant phase element (CPE), with parameters *Q* and *a*, corresponds to a distributed capacitive contribution of the network, indicating an imperfect dielectric behavior.[25] The parallel capacitive term, *C*, is attributed to the contribution of the electrodes.[24] The fact that the Nyquist plot could be modeled without an additional resistor in parallel to the CPE suggests that polarization resistance in the network is negligible.

The networks' electrical characteristics were quantitatively compared by the values of the equivalent circuit components (**Table 1**). A 2.5 fold decrease in the network bulk resistance was observed once the filaments have been aged for one week before deposition. This effect was accompanied by a 3 fold increase in *Q*. We note that for the reference bare sample *R* was ~3 orders of magnitude larger, and *Q* was found to be substantially smaller (Figures 2b and S3, and Table 1), indicating that once peptide fibrils are deposited, charge transport occurs through the network itself. *C* retained almost the same value in all cases, suggesting that the capacitance is limited by the geometrical capacitance of the electrodes system.[26]

Both DC and AC measurements indicate that the network resistance is strongly dependent on its folding state (Figures 2 and S4). This behavior could be explained by an increase in the charge transport rate due to the formation of additional, or more efficient, hydrogen bond bridges for β sheets folded into fibrils. Alternatively, it may indicate on higher charge density in the fibril form. Overall, these results indicate that the resistance can be modulated by controlling the conformation of the structure. However further studies are required to fully uncover this effect. While the AC and DC data exhibited similar trends, the DC resistance values were found to be one order of magnitude higher than the AC values. This is despite of the slightly higher relative humidity in the DC measurements. This behavior is attributed to the blocking nature of the gold electrodes, which is evident in the impedance measurements by the low frequency slope. Hence, a large contact resistance increases the measured DC values. However, it is important to note that these results suggest that despite proton blocking, the measured DC currents under high relative humidity originate from protonic transport through the peptide networks.

2.3. Dependence of Electrical Characteristics on Relative Humidity

Equation (1) implies that protonic conductivity, which depends linearly on charge carriers' concentration, should increase exponentially with the relative humidity. Indeed, an abrupt increase in the DC current with increasing relative humidity was observed for both aged and fresh peptide fibril networks in the

Table 1. Equivalent circuit parameters of freshly prepared and aged peptide networks, and a reference bare chip, at different relative humidity conditions.

Relative humidity	Solution aging time	Equivalent electric circuit element[a)]			
		R [GΩ]	Q [nF·sec^{a-1}]	*a*	C [nF]
75%	one week	0.04 ± 0.01	15 ± 3	0.35 ± 0.04	0.300 ± 0.003
75%	fresh solution	0.100 ± 0.006	5 ± 1.4	0.40 ± 0.05	0.300 ± 0.001
75%	bare chip	25 ± 10	0.1 ± 0.1	0.39 ± 0.03	0.250 ± 0.002
30%	one week	120 ± 20	0.4 ± 0.1	0.77 ± 0.04	0.270 ± 0.001
vacuum	one week	300 ± 150	–	–	0.220 ± 0.003

[a)]Data was obtained by fitting the Nyquist plots presented in Figures 2b and 3c using the equivalent circuit presented in Figure 2b.

range of 30-86% relative humidity (**Figures 3**a and S5, respectively). An exponential dependence of the conductance on the relative humidity was observed at the high relative humidity range (Figure 3b). Such behavior was observed for oxides,[20e] synthetic polymers,[27] DNA,[19a,20b,21,28] and proteins,[2b,11e,22,29] and was attributed to protonic conduction. However, our data indicated, unexpectedly, a bimodal exponential dependence of the conductance on the relative humidity for both peptide samples, with lower values for the freshly prepared samples, for the entire relative humidity range (Figure 3b). In particular, a moderate dependence of the conductance on the relative humidity was found below 60% relative humidity, with an exponential pre-factor of 0.0964 ± 0.0001 and 0.068 ± 0.003 for the aged and un-aged networks, respectively. An abrupt increase in the dependence was found above 60% relative humidity for both freshly prepared and aged networks, with exponential pre-factors of 0.127 ± 0.002 and 0.17± 0.02, respectively. While such bimodal behavior may have been attributed to invoking transport by residual ions,[22] the involvement of ions in the conduction for these samples under the used measurement conditions has been ruled out,[11e] as discussed above.

In order to rule out substrate effects, the conductance of bare chips, before peptide network deposition, was measured under the same conditions. The conductance, which is attributed to proton transport across the hydroxylated oxide surface,[30] was found to be always lower by at least 30% for the reference bare chip measurements (Figure 3b). In this case a single exponential dependence of the conductance on the relative humidity was observed for the entire relative humidity range. These protonic currents dropped below the measurement sensitivity level under the entire relative humidity range by capping the free hydroxyl groups by silanization with triethoxy(octyl)silane (Figure S6). Conduction could be recovered on such silanized chips once a network of the peptide was drop- casted on the surface (Figure S6). These results indicate that the observed bimodal behavior can be attributed to the peptide network itself and not to the substrate. The observed behavior is not restricted to the thienylalanine containing networks; *I–V* measurements obtained for a network of fibrils self-assembled from a peptide with the sequence AAKLVFF indicated similar conductance – relative humidity trends (Figure S7). Under lower relative humidity values a relatively small increase in the conductance was observed with increasing relative humidity. A much higher dependence on the relative humidity was observed for relative humidity above 50%. Hence, these results indicate that the bimodal conductance behavior is an intrinsic property of the peptide network.

Changes in the conductance should be reflected in the impedance characteristics as well. Indeed, repeating the

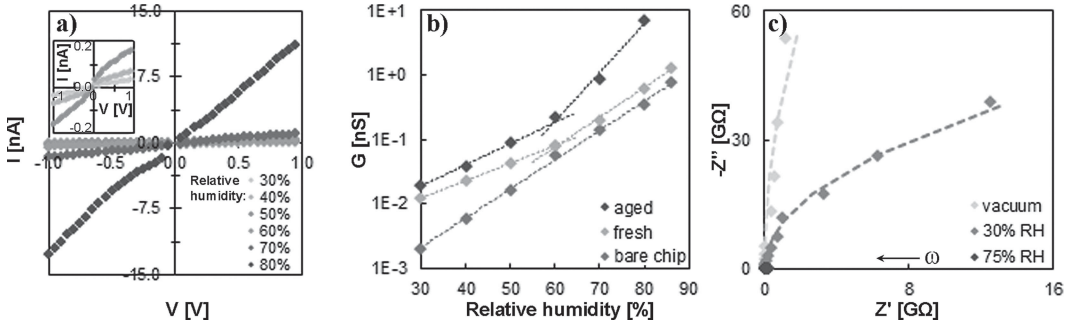

Figure 3. Dependence of electrical behavior on relative humidity. a) *I–V* curves measured under different relative humidity conditions of a sample prepared from an aged peptide solution. Measurements were recorded on chips with 500 μm wide electrodes. Zoom on the *I–V* curves recorded at the lower relative humidity range appears in the inset. b) Conductance values extracted from the slope of *I–V* curves as function of the relative humidity for peptide networks drop- casted from fresh and one week aged peptide solutions and for a bare reference chip after Piranha treatment. Data of sample prepared from an aged solution was normalized by a factor of 0.6 in order to compare with results of other samples that were recorded on chips with 300 μm wide electrodes. Errors in conductance values are ~1% for the entire relative humidity range. Fitting of the data is shown by dashed lines, revealing bimodal exponential dependence of the conductance on the relative humidity for the peptide networks, and a single exponent dependence for the clean chip. c) Impedance Nyquist plots of peptide network prepared from one week aged solution under different relative humidity conditions. Dashed lines represent the fitting results. Zoom on the results of measurements conducted at 75% relative humidity is shown in Figure 2b.

impedance spectroscopy measurements at lower relative humidity conditions of 30%, and also under low vacuum of 10^{-3} mbar (Figures 3c and S8), indicated remarkable differences. One incomplete semicircle was observed in the Nyquist plot obtained under lower relative humidity conditions, indicating remarkable increase in the resistance. A similar behavior was observed for a different peptide nanotube network.[6c] Indeed, for the aged network R was found to increase by more than three orders of magnitude once the humidity decreased from 75% to 30% (Table 1), as predicted by the exponential dependence of protonic conductance on the relative humidity (Equation (1), and observed in the DC measurements presented above). In addition to the substantial increase in R, Q has decreased by 2 orders of magnitude, and was accompanied by an increase in a (Table 1), indicating a less significant, but more homogeneous capacitive contribution. Furthermore, as observed in the DC measurements, further reduction of the relative humidity by pumping the system resulted in only a threefold increase in R (Table 1). In particular, under vacuum the data could be fitted to a simple parallel RC circuit. Similar results were obtained for the fresh sample (Figure S8), albeit with higher resistance values. Interestingly, in contrast to the behavior under elevated relative humidity, under lower relative humidity conditions a much better agreement was obtained between the DC and AC resistance values (Figure S4), with only twofold difference between resistance values as compared to one order of magnitude difference at higher relative humidity. This indicates that the serially connected resistance that limits the DC conductance under elevated relative humidity, which was attributed to the proton blocking nature of the gold electrodes, is less dominant under the lower humidity values. Overall, these results further indicate that the decrease in protonic bulk conductance due to humidity dependent reduction in the density of charge carriers (Equation (1)), invokes another conduction mechanism, which is less dependent on the humidity. A crossover point between these two mechanisms occurs at a relative humidity of approximately 60% (Figure 3b).

2.4. Temporal Current Behavior at Low Relative Humidity

The smaller dependence of the conductance on the humidity at the low relative humidity range may be explained by a humidity insensitive mechanism of proton conduction through a single water adlayer.[19a] However, electron transport may also result in sub-exponential dependence of the conductance on the humidity.[31] In order to validate the contribution of electrons to the conduction at the low relative humidity range, transient current measurements were carried out under vacuum conditions (**Figure 4**a). It was speculated that under such conditions proton contribution to the conduction would diminish with time due to exhaustion of charge carriers' source, while electronic conduction would retain a constant value due to electron supply from the gold electrodes.[11b,32] An abrupt increase in the current from 0 to 2.5 pA was observed upon switching the applied voltage from 0 to 3 V. We note that water hydrolysis was found to be negligible at this voltage, as apparent by the linear behavior of the I–V relations (data not shown).[21] This was followed by a rapid current decrease for the first few minutes, followed by a more gradual decrease in the current for twenty five minutes. Fitting the data indicated that the current decays exponentially with two different time constants of 0.95 and 10 minutes (Figure 4a). The shorter time constant of 0.95 minutes was found to be in agreement with the RC time of the equivalent circuit, τ_{RC} = 1.13 minutes, as calculated from the impedance data (Table 1). The longer decay time is hence attributed to proton transport that, as expected, reduces with time. We note

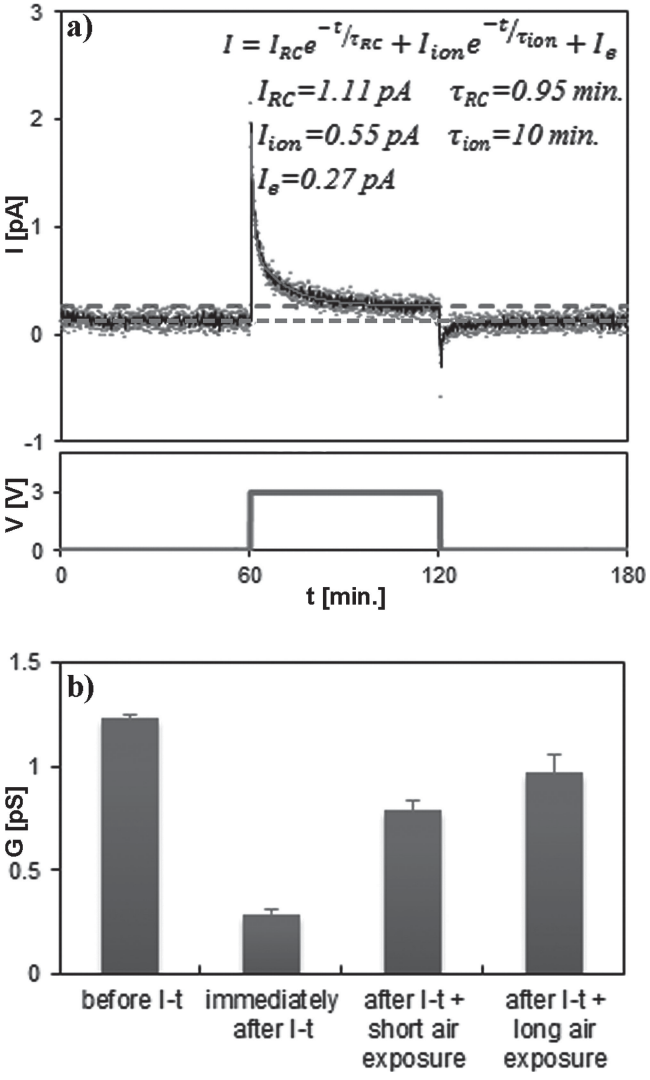

Figure 4. Aged peptide network transient current. a) Transient current measurement of a sample prepared from an aged peptide solution under vacuum ($P = 10^{-4}$ mbar). Raw data is plotted in light gray, with moving average flattened values represented in dark gray. Black line shows the fitting of the data between 60-120 minutes. Gray dotted line indicates the baseline current under 3V. Gray dashed line indicates the zero voltage current (which is not zero due to an offset of the measurement instrument). Measurements were recorded on chips with 500 μm wide electrodes. Lower currents were measured compared to the I–V measurements presented above, probably due to a smaller amount of material between the electrodes. b) Conductance values under vacuum conditions obtained before and immediately after the experiments, after a short exposure to air (~15 minutes) and pumping back to vacuum, and after a longer exposure to air (~24 h) and pumping back to vacuum. Errors in conductance were estimated as the fitting error of the I–V curves.

that switching the applied bias back to zero after 1 hour at 3 V resulted in an abrupt decrease of the current to –0.6 pA, followed by a rapid increase of 3 minutes back to ~0.1 pA (which represents a zero current taking into account an internal offset of the measurement instrument), presenting only the RC transient response. No response was observed for a clean reference chip without peptide network under the same transient conditions (data not shown), indicating that the observed behavior cannot be attributed to stray capacitance effects from the leads or substrate. Hence, we conclude that proton transport can be invoked even under vacuum, probably due to the presence of a single or partial water adlayer surrounding the peptide.

Importantly, after twenty five minutes at 3 V, the current stabilized at a value of ~0.3 pA, indicating that a constant flow of electrons exists in the system. Therefore, our results indicate that under low humidity conditions hybrid proton and electron conduction is manifested in the peptide fibril networks. Exponential fit of our results suggests that at the voltage onset time the protonic current is twice as large as the electron current for the studied peptide network under vacuum conditions (Figure 4a). We note that such hybrid conduction process was suggested recently to explain electronic behavior of melanin.[31] For the peptide networks this hybrid conduction can explain the better agreement in the DC and AC resistance values observed at the low humidity range (Figure S4); while at the higher humidity range for which conduction is dominated by protons, the blocking nature of the gold electrode introduces a resistance term in series to the bulk resistance, making the DC resistance much higher, this term is less dominant at the lower humidity range since the conduction is obtained partially by electron transport with smaller electrode contact resistance.

Further indication for the hybrid protonic and electronic conduction was obtained by monitoring the conductance under vacuum before and after the transient measurement (Figure 4b). Before the transient, conductance of ~1.2 pS was measured. This value decreased to ~0.3 pS immediately after the transient experiment, as could be expected from the deficiency in protonic charge carriers. An increase in the conductance to ~0.8 pS was measured in vacuum after exposing the sample to air for a short time of about 15 minutes. Further exposure to air for about 24 hours, resulted in almost a full recovery of the low pressure conductance to the initial value measured before the transient. These results further confirm the contribution of water molecules to the conduction even under vacuum conditions. The slow recovery time may indicate a slow reformation of the water adlayer. The recovery of the current further indicates that the reduction in the current observed during the transient cannot be attributed to irreversible physical damage to the peptide fibrils. It should, however, be noted that reversible conformational changes due to the depletion of water could occur. Our results, hence, clearly indicate hybrid electron and proton conduction at the low humidity range. It should be noted that both type of conduction mechanisms can contribute to the sub-exponential dependence below 60% relative humidity crossover point; on the one hand, dielectric theories predict some dependence of electron transport on humidity,[11c,11d,31], [33] while on the other hand the more gradual increase in the conductance at the lower humidity range can be attributed to dominance of H_3O^+ and not H^+ on protonic conductance.[19a,20a] The relative contribution of each type of charge carrier to the conductance at the entire relative humidity range should be further investigated.

Finally, we would like to note that the conductance was found to be much lower for the fibril network of the AAKLVFF peptide for the entire relative humidity measurement range (Figure S7). While this could be expected under the low relative humidity range, for which electronic conduction is expected to be higher for (2-Thi)(2-Thi)VLKAA network due to the introduction of thiophene instead of phenyl side chains,[8] the improved conduction under higher relative humidity values, indicates that the exchange of the phenyl groups with thiophenes affects also the protonic conductance. These differences could be attributed to subtle changes in the structure of the filaments, which influence proton transport (by changes in its mobility). However, further investigations are required in order to understand this behavior.

3. Conclusions

Detailed AC and DC characterization of the electrical behavior of peptide fibril networks under a large relative humidity range revealed a hybrid electron and proton transport in peptide filaments. This hybrid behavior leads to a bimodal exponential dependence of the conductance on the relative humidity with a crossover point at ~60% relative humidity. Below the crossover point both electrons and protons contribute to the conduction, with the latter contribution persisting even under vacuum conditions. This results in a smaller dependence of the conduction on the relative humidity. Above the crossover point, proton transport becomes the dominant conduction mechanism with a much higher dependence of conductance on the relative humidity. At such higher relative humidity values, the network behaves like a porous protonic conductor. Furthermore, both the conduction and the exponential dependence on the relative humidity are affected by the extent of folding of the peptide network. In particular, the conductance is higher for fully folded peptide fibers, demonstrating the possible effects the conformation of the structure may have on both types of conduction mechanisms. However, due to the different chemical nature of electron and proton conducting ligands, the conduction by each of the charge carriers may be tuned individually by a proper peptide sequence design. Our findings demonstrate that peptide based materials can be used either as electronic or protonic electric and optoelectronic devices.

4. Experimental Section

Peptide Synthesis: A peptide with the sequence (2-Thi)(2-Thi)VLKAA was synthesized by standard Fmoc solid phase synthesis methods, as described elsewhere,[18] and used as a trifluoroacetic acid salt. The purity of the peptide was verified by high-performance liquid chromatography (HPLC), and was found to be above 93%.

Sample Preparation: 300 μm wide/1 μm thick or 500 μm wide/100 nm thick gold electrodes, with 20 μm gaps were fabricated on silicon wafers with a top 100 nm silicon-oxide layer. 10 nm Ti adhesion layer was used for the deposition of gold. Electrode chips consisted of 7/6 pairs of electrodes for the first/second chip configuration, respectively, allowing multiplication of experiments for each type of sample.

Prior to peptide network deposition chips were cleaned using freshly prepared Piranha solution (solution of 3:7 30% H_2O_2 and concentrated H_2SO_4) for 20-30 minutes (Caution: Piranha is a very strong oxidant and reacts violently with many organic materials), washed three times in triply distilled water (TDW, 18.2 MΩ, EASYpure®RoDi -Thermo Scientific, USA), and dried under a nitrogen flow. Self-assembled peptide fibril networks were prepared by drop- casting 10 µl of peptide solutions (0.3 mM) in Methanol (HPLC grade A, Sigma Aldrich). Samples were left to dry overnight prior to electrical characterizations. For the characterization of aged samples the peptide solution was aged for one week in solution prior to the drop - casting process, in order to assure complete folding of the peptide into fibers. Scanning electron microscopy (SEM) characterizations were obtained on samples prepared in a similar manner on a bare silicon wafer.

Silanized samples were prepared by placing Piranha treated chips in a closed container in the presence of 1 ml drops of Triethoxy(octyl)silane (TEOS, Sigma-Aldrich). TEOS was allowed to evaporate and deposit on the sample for 30 minutes. Excess material was washed with ethanol. Samples were then dried under a nitrogen flow, followed by 1 h curing at 120 °C. Contact wetting angles were measured using KRÜSS EasyDrop apparatus.

Morphological Characterization: Atomic force microscopy (AFM, Solver-Pro, NT-MDT, Ru) topography images were acquired in tapping mode using non-contact tips (BudgetSensors Multi75Al-G (3 N/m, 75 kHz)). Cross section measurements and image processing, which included second order polynomial line fitting, were done using the NOVA AFM software. SEM images were performed using a high resolution scanning electron microscopy (HRSEM, JEOL JSM-7400F, Japan).

Electrical Characterization: Current-voltage (*I–V*) measurements were acquired using a probe station (JANIS research co., Inc., U.S.A) connected to a Keithley 2635 Source-Meter unit in a two electrodes configuration. All measurements were carried out from 0 V to ±1 V with 0.05 V steps, and 1 sec sweep delay. Since the behavior of the *I–V* appeared to be linear through the entire relative humidity range, conductance values were extracted from the slope of the linear-fitted curves, using the Origin software. Conductance was evaluated by averaging values of at least 5 different electrodes in each chip and the error was calculated as the standard deviation, resulting in an estimated error of ~1% in humidified atmosphere, and ~4% under vacuum conditions. High reproducibility was obtained for experiments conducted on different electrodes on the same chip, and for experiments conducted on different chips. Moreover, no degradation in the current was observed for samples stored for about two months. Transient current measurements (*I–t*) were conducted using the same measurement configuration under vacuum conditions ($P = 10^{-4}$ mbar), applying constant voltages of 0, – 3 and 0 V for 1 h interval at each voltage, with data points recorded every 5 seconds. *I–V* measurements before and after the transient current experiment were carried out from 0 V to 3 V with 0.1 V steps, and 1 sec sweep delay. Solid-state impedance spectroscopy measurements were carried out in the same probe station, using a Solartron 1260 frequency response analyzer and Solartron 1296 dielectric interface. Impedance spectra were measured over a frequency range of 10 mHz to 32 MHz, with DC level of 0 V and AC amplitude of 100 mV. Equivalent electric circuit fitting was done using EC-Lab (BioLogic) software. The relative humidity of the environment was controlled during the measurements in the range of 30-86% relative humidity using a home-made system that controls separately the flow of dry and humidified nitrogen into the measurement chamber. To achieve minimum humidity, measurements were conducted under vacuum at a pressure of 10^{-4} –10^{-3} mbar achieved using a BOC EDWARDS XDD1 diaphragm pump and EXT75DX compound molecular pump with Turbo pump. Changes in the conductance occurred almost immediately after the relative humidity change, and were reproducibly obtained upon changing from high to low relative humidity values, and *vice versa*.

Supporting Information

Supporting Information is available from the Wiley Online Library or from the author.

Acknowledgements

This research was supported by a grant from the Israel Science Foundation (1293/08), and the Edmond J. Safra Foundation through the Biopolymers Center. M.A. is a recipient of the Converging Technology Fellowship of the Planning and Budgeting Committee, the Council for Higher Education, Israel, and the Kreitman Fellowship for doctoral research. Electrodes were fabricated at the Weiss Family Laboratory for Nano-Scale Systems at the Ben-Gurion University of the Negev and at the Unit for Nanofabrication at the Hebrew University of Jerusalem. We are grateful to Prof. Aleman from Universitat Politècnica de Catalunya (Spain) for his contribution to this work.

Received: April 7, 2014
Revised: May 19, 2014
Published online: July 14, 2014

[1] a) J. Lewis, *Mater. Today* **2006**, *9*, 38; b) S. Park, M. Vosguerichian, Z. Bao, *Nanoscale* **2013**, *5*, 1727; c) M. Kaltenbrunner, T. Sekitani, J. Reeder, T. Yokota, K. Kuribara, T. Tokuhara, M. Drack, R. Schwodiauer, I. Graz, S. Bauer-Gogonea, S. Bauer, T. Someya, *Nature* **2013**, *499*, 458.

[2] a) G. Maruccio, A. Biasco, P. Visconti, A. Bramanti, P. P. Pompa, F. Calabi, R. Cingolani, R. Rinaldi, S. Corni, R. Di Felice, E. Molinari, M. R. Verbeet, G. W. Canters, *Adv. Mater.* **2005**, *17*, 816; b) P. P. Pompa, A. Della Torre, L. L. del Mercato, R. Chiuri, A. Bramanti, F. Calabi, G. Maruccio, R. Cingolani, R. Rinaldi, *J. Chem. Phys.* **2006**, *125*, 021103; c) E. D. Mentovich, B. Belgorodsky, I. Kalifa, H. Cohen, S. Richter, *Nano Lett.* **2009**, *9*, 1296; d) D. Li, P. M. Gannett, D. Lederman, *Nanotechnology* **2012**, *23*, 395705.

[3] a) J. J. Davis, D. A. Morgan, C. L. Wrathmell, D. N. Axford, J. Zhao, N. Wang, *J. Mater. Chem.* **2005**, *15*, 2160; b) G. Maruccio, P. Marzo, R. Krahne, A. Passaseo, R. Cingolani, R. Rinaldi, *Small* **2007**, *3*, 1184; c) I. Ron, I. Pecht, M. Sheves, D. Cahen, *Acc. Chem. Res.* **2010**, *43*, 945; d) E. A. Della Pia, M. Elliott, D. D. Jones, J. E. Macdonald, *ACS Nano* **2012**, *6*, 355; e) J. E. Jett, D. Lederman, L. A. Wollenberg, D. Li, D. R. Flora, C. D. Bostick, T. S. Tracy, P. M. Gannett, *J. Am. Chem. Soc.* **2013**, *135*, 3834.

[4] a) S. Yasutomi, T. Morita, Y. Imanishi, S. Kimura, *Science* **2004**, *304*, 1944; b) S. Sek, K. Swiatek, A. Misicka, *J. Phys. Chem. B* **2005**, *109*, 23121; c) K. Takeda, T. Morita, S. Kimura, *J. Phys. Chem. B* **2008**, *112*, 12840; d) Y. Arikuma, H. Nakayama, T. Morita, S. Kimura, *Angew. Chem., Int. Ed.* **2010**, *49*, 1800.

[5] C. Shlizerman, A. Atanassov, I. Berkovich, G. Ashkenasy, N. Ashkenasy, *J. Am. Chem. Soc.* **2010**, *132*, 5070.

[6] a) L. L. del Mercato, P. P. Pompa, G. Maruccio, A. Della Torre, S. Sabella, A. M. Tamburro, R. Cingolani, R. Rinaldi, *Proc. Natl. Acad. Sci. USA* **2007**, *104*, 18019; b) J. Castillo, S. Tanzi, M. Dimaki, W. Svendsen, *Electrophoresis* **2008**, *29*, 5026; c) H. Xu, A. K. Das, M. Horie, M. S. Shaik, A. M. Smith, Y. Luo, X. Lu, R. Collins, S. Y. Liem, A. Song, P. L. A. Popelier, M. L. Turner, P. Xiao, I. A. Kinloch, R. V. Ulijn, *Nanoscale* **2010**, *2*, 960; d) M. Mizrahi, A. Zakrassov, J. Lerner-Yardeni, N. Ashkenasy, *Nanoscale* **2012**, *4*, 518.

[7] N. Ashkenasy, W. S. Horne, M. R. Ghadiri, *Small* **2006**, *2*, 99.

[8] M. Amit, G. Cheng, I. W. Hamley, N. Ashkenasy, *Soft Matter* **2012**, *8*, 8690.

[9] a) I. F. Perepichka, D. F. Perepichka, H. Meng, F. Wudl, *Adv. Mater.* **2005**, *17*, 2281; b) C. B. Nielsen, I. McCulloch, *Prog. Polym. Sci.* **2013**, *38*, 2053.
[10] S. Cukierman, *BBA-Bioenergetics* **2006**, *1757*, 876.
[11] a) M. H. Cardew, D. D. Eley, *Discuss. Faraday Soc.* **1959**, *27*, 115; b) B. Rosenberg, *Nature* **1962**, *193*, 364; c) B. Rosenberg, E. Postow, *Ann. NY Acad. Sci.* **1969**, *158*, 161; d) M. Powell, B. Rosenberg, *J. Bioenerg.* **1970**, *1*, 493; e) H. Morgan, R. Pethig, *J. Chem. Soc., Farad. Trans. 1* **1986**, *82*, 143.
[12] P. Meredith, C. J. Bettinger, M. Irimia-Vladu, A. B. Mostert, P. E. Schwenn, *Rep. Prog. Phys.* **2013**, *76*, 034501.
[13] J. D. Tovar, *Acc. Chem. Res.* **2013**, *46*, 1527.
[14] a) Y. J. Kang, S.-J. Chun, S.-S. Lee, B.-Y. Kim, J. H. Kim, H. Chung, S.-Y. Lee, W. Kim, *ACS Nano* **2012**, *6*, 6400; b) X. Zhang, Z. Lin, B. Chen, S. Sharma, C.-p. Wong, W. Zhang, Y. Deng, *J. Mater. Chem. A* **2013**, *1*, 5835.
[15] a) S. Xin, Y.-G. Guo, L.-J. Wan, *Acc. Chem. Res.* **2012**, *45*, 1759; b) L. M. Zhu, A. W. Lei, Y. L. Cao, X. P. Ai, H. X. Yang, *Chem. Commun.* **2013**, *49*, 567.
[16] a) Y. A. Elabd, M. A. Hickner, *Macromolecules* **2011**, *44*, 1; b) L. Wu, Z. Zhang, J. Ran, D. Zhou, C. Li, T. Xu, *Phys. Chem. Chem. Phys.* **2013**, *15*, 4870.
[17] a) C. Zhong, Y. Deng, A. F. Roudsari, A. Kapetanovic, M. P. Anantram, M. Rolandi, *Nat. Commun.* **2011**, *2*, 476; b) Y. Deng, E. Josberger, J. Jin, A. F. Rousdari, B. A. Helms, C. Zhong, M. P. Anantram, M. Rolandi, *Sci. Rep.* **2013**, *3*, 2481.
[18] I. W. Hamley, G. D. Brown, V. Castelletto, G. Cheng, M. Venanzi, M. Caruso, E. Placidi, C. Aleman, G. Revilla-López, D. Zanuy, *J. Phys. Chem. B* **2010**, *114*, 10674.
[19] a) D. H. Ha, H. Nham, K. H. Yoo, H. M. So, H. Y. Lee, T. Kawai, *Chem. Phys. Lett.* **2002**, *355*, 405; b) M. E. Tuckerman, D. Marx, M. Parrinello, *Nature* **2002**, *417*, 925; c) R. Ludwig, *Angew. Chem., Int. Ed.* **2003**, *42*, 258.
[20] a) J. H. Anderson, G. A. Parks, *J. Phys. Chem.* **1968**, *72*, 3662; b) C. Yamahata, D. Collard, T. Takekawa, M. Kumemura, G. Hashiguchi, H. Fujita, *Biophys. J.* **2008**, *94*, 63.
[21] T. Kleine-Ostmann, C. Jordens, K. Baaske, T. Weimann, M. H. de Angelis, M. Koch, *Appl. Phys. Lett.* **2006**, *88*, 102102.
[22] G. H. Bardelmeyer, *Biopolymers* **1973**, *12*, 2289.
[23] J. T. S. Irvine, D. C. Sinclair, A. R. West, *Adv. Mater.* **1990**, *2*, 132.
[24] L. Garrido, M. López-González, M. Tlenkopatchev, E. Riande, *J. Membr. Sci.* **2011**, *380*, 199.
[25] J. R. Macdonald, Ed., *Impedance Spectroscopy: Emphasizing Solid Materials and Systems*, Wiley, New York, USA, **1987**.
[26] N. J. Kidner, Z. J. Homrighaus, B. J. Ingram, T. O. Mason, E. J. Garboczi, *J. Electroceram.* **2005**, *14*, 283.
[27] a) E. S. Matveeva, *Synth. Met.* **1996**, *79*, 127; b) J. H. Christie, S. H. Krenek, I. M. Woodhead, *Biosyst. Eng.* **2009**, *102*, 143.
[28] B. Skinner, M. S. Loth, B. I. Shklovksii, *Phys. Rev. E* **2009**, *80*, 041925.
[29] B. Rosenberg, *J. Chem. Phys.* **1962**, *36*, 816.
[30] a) J. A. Voorthuyzen, K. Keskin, P. Bergveld, *Surf. Sci.* **1987**, *187*, 201; b) S. H. Song, H. H. Yang, C. H. Han, S. D. Ko, S. H. Lee, J. B. Yoon, *Appl. Phys. Lett.* **2012**, *100*, 101603.
[31] A. B. Mostert, B. J. Powell, F. L. Pratt, G. R. Hanson, T. Sarna, I. R. Gentle, P. Meredith, *Proc. Natl. Acad. Sci. USA* **2012**, *109*, 8943.
[32] M. S. Mattsson, G. A. Niklasson, *J. Appl. Phys.* **1999**, *85*, 8199.
[33] T. Andrade-Filho, F. F. Ferreira, W. A. Alves, A. R. Rocha, *Phys. Chem. Chem. Phys.* **2013**, *15*, 7555.